Physica D 402 (2020) 132256

Contents lists available at ScienceDirect

Physica D

journal homepage: www.elsevier.com/locate/physd

Understanding the order-chaos-order transition in the planar elastic pendulum

Anurag [a,*], Basudeb Mondal [b], Jayanta K. Bhattacharjee [c], Sagar Chakraborty [a]

[a] Department of Physics, Indian Institute of Technology Kanpur, Uttar Pradesh 208016, India
[b] International Centre for Theoretical Sciences, Tata Institute of Fundamental Research, Bangalore 560089, India
[c] Department of Theoretical Physics, IACS, 2A & 2B Raja S. C. Mullick Road, Kolkata 700032, India

ARTICLE INFO

Article history:
Received 9 January 2019
Received in revised form 15 October 2019
Accepted 31 October 2019
Available online 11 November 2019
Communicated by I. Melbourne

Keywords:
Hamiltonian systems
Nonintegrable systems
Order-chaos-order transition
Chirikov criterion
Swinging spring pendulum

ABSTRACT

A planar elastic pendulum can be thought of as a planar simple pendulum and a one-dimensional Hookian spring carrying a point mass coupled together nonlinearly. This autonomous nonintegrable Hamiltonian system shows autoparametric resonance that corresponds to the 2 : 1 primary resonance in the nearly integrable Hamiltonian approximating the planar elastic pendulum's full Hamiltonian. The system is also known to exhibit the phenomenon of the order-chaos-order in which the system transits from a predominantly ordered state to a chaotic state and then back to a predominantly regular state. Although there are well-documented numerical experiments reporting that the system is most chaotic around the condition of autoparametric resonance, the exact mechanism behind the order-chaos-order transition sandwiching the aforementioned chaotic state is not completely understood. In this paper, by employing a combination of analytical and numerical methods, we establish that the order-chaos-order transition occurs due to the interaction between two 2 : 1 resonances—one primary and another secondary.

1. Introduction

It is very fascinating that deceptive simplicity of low-degree-of-freedom systems, like elastic pendulum (also called swing–spring [1]) – a three-degrees-of-freedom Hamiltonian system – still intrigues researchers with newer phenomena even though more than three centuries have elapsed since the governing equations of the elastic pendulum have been established. Needless to say that quantum version of the elastic pendulum is equally interesting; practically speaking, the pendulum models the quantum dynamics of a few triatomic molecules, e.g., CO_2, where stretching of the molecular bonds and bending of the molecule can be thought to be mimicked by the elastic pendulum's springing motion and the pendulum's swinging motion respectively. One rather newly found phenomenon in the elastic pendulum is that of Hamiltonian monodromy [2–6]. The phenomenon of order-chaos-order [7–11] is yet another interesting phenomenon seen in the *planar* elastic pendulum (PEP) [10,12–22], an even simpler version of the elastic pendulum, where the elastic pendulum is constrained to oscillate in a fixed vertical plane as shown in Fig. 1. In the phenomenon of the order-chaos-order, the system switches between the states of the widespread chaotic motion and the predominantly regular motion. The PEP has also been used as a prototype model to illustrate that the seed of irreversibility exists in the complex dynamics of the nonlinear conservative system of merely two-degrees-of-freedom [23].

To understand the precise meaning of the order-chaos-order phenomenon, we recall [24] that a nonintegrable autonomous Hamiltonian system possesses some chaotic trajectories even if the nonlinearity is very weak. These trajectories for two-degrees-of-freedom systems are localized between two KAM tori [25–27]; for a higher degree of freedom systems, however, Arnold diffusion [28] can overcome this confinement of the trajectories. Somewhat figuratively speaking, when the boundaries of two such localized regions come in contact with each other as some system-parameter changes, the localized chaos gives way to the widespread chaos. The Chirikov resonance overlap criterion [29] gives an approximate quantitative estimate regarding when the transition between the local chaos and the widespread chaos in the system occurs. The criterion is based on the idea that it is the overlap of two independent resonances that leads to the widespread chaos. In the widespread chaotic regime, it is rather easy to observe chaotic motion. In contrast, in the local chaotic regime, the motion would appear predominantly regular.

In fact, although not probably reported in the literature, we believe that the order-chaos-order phenomenon might be present

* Corresponding author.
E-mail addresses: anuragsh@iitk.ac.in (Anurag), basudeb.mondal@icts.res.in (B. Mondal), tpjkb@iacs.res.in (J.K. Bhattacharjee), sagarc@iitk.ac.in (S. Chakraborty).

https://doi.org/10.1016/j.physd.2019.132256
0167-2789/

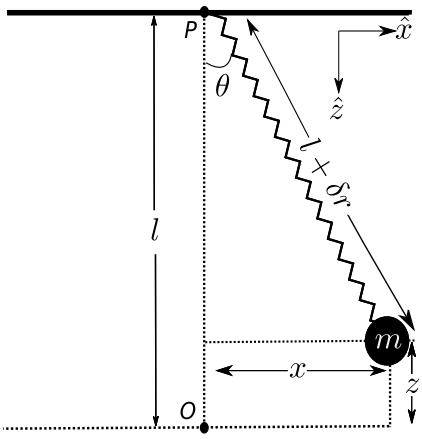

Fig. 1. *A schematic diagram of the planar elastic pendulum (PEP). P* is the immovable rigid point of support of the PEP and point *O* is the equilibrium point at which $mg = k_s(l - l_0)$. (See Section 1 for the details.)

in the elastic pendulum as well: In the limit of very stiff spring, the elastic pendulum would appear as a spherical pendulum that is known as to be integrable [30], and hence, is expected to show mostly regular ordered motion. On the other hand, in the limit of small amplitude motion, the nonlinear coupling between the springing motion and the swinging motion can be taken to be so small that the dynamics of the elastic pendulum would correspond to the uncoupled integrable motions of a spherical pendulum and a Hookian spring carrying a point mass at one end. Thus, we do expect the nonintegrable elastic pendulum [31] to show widespread chaos for the other ranges of parameters, and hence, the order-chaos-order phenomenon.

The numerical search for the order-chaos-order transition is quite straightforward, but that does not reveal the mechanism behind this phenomenon. Moreover, since dealing with a fully nonintegrable Hamiltonian analytically is almost impossible, it would be quite insightful if appropriate perturbative methods could be invoked to comprehend the phenomenon of order-chaos-order. To the best of our knowledge, this endeavour has not been taken up yet in the literature. Thus, in this paper, we are motivated to investigate the phenomenon of the order-chaos-order by considering the example of the PEP that is a two-degrees-of-freedom autonomous nonintegrable Hamiltonian system consisting of a point mass attached to the free end of a massless elastic or extensible spring and is constrained to oscillate in a vertical plane (see Fig. 1).

The Hamiltonian of the PEP in the radial–polar coordinate system is given by [10,12],

$$H = \frac{p_r^2}{2m} + \frac{p_\theta^2}{2m(\delta r + l)^2} + \frac{1}{2}k_s\delta r^2 + mg\delta r(1 - \cos\theta) + mgl(1 - \cos\theta) + E_{\min}\,, \tag{1}$$

where m is the mass attached with the spring, k_s is the spring constant, g is the acceleration due to gravity acting downwards, δr and θ are the radial and the polar coordinates respectively, and p_r and p_θ are the corresponding conjugate momenta. $E_{\min} \equiv -mgl + m^2g^2/2k_s$ is the minimum energy of the PEP, i.e., the energy when it is at rest and l is the equilibrium length of the spring. For future convenience, we define, $H \equiv -RE_{\min}$, $\omega_s^0 \equiv \sqrt{k_s/m}$, $\omega_p^0 \equiv \sqrt{g/l}$ and $\mu \equiv (\omega_s^0/\omega_p^0)^2 = 1 + k_s l_0/mg \geq 1$, where l_0 is the rest length of the spring. In this paper, we fix $m = 1$, $k_s = 100$, and $g = 9.81$—all in the S.I. units.

For small values of μ, i.e., $\mu \to 1$, the coupling between the radial (springing) and the angular (swinging) modes of the PEP is weak, and so the phase space trajectories are mostly regular [10]. For large values of μ, we can argue that k_s is large (hard spring) so that the spring behaves like an inextensible string, and hence most of the energy is in angular mode making the system effectively a one-degree-of-freedom pendulum system. Thus, the phase space trajectories for the large value of μ are again regular. Hence, it intuitively appears that there may be an order-chaos-order transition in the PEP. In fact, Fig. 2 illustrates that the Poincaré sections of the PEP in libration regime at $R = -0.7$ and rotation regime at $R = 4.0$ for different values of μ speak volumes for the existence of the order-chaos-order phenomenon in both the libration and the rotation regimes. In general, while the libration or the rotation states depend both on the values of R and μ, it can be shown [10] that for $R < 0$ and $R > 1$, the system is in the libration and the rotation regimes respectively for any allowed value of μ.

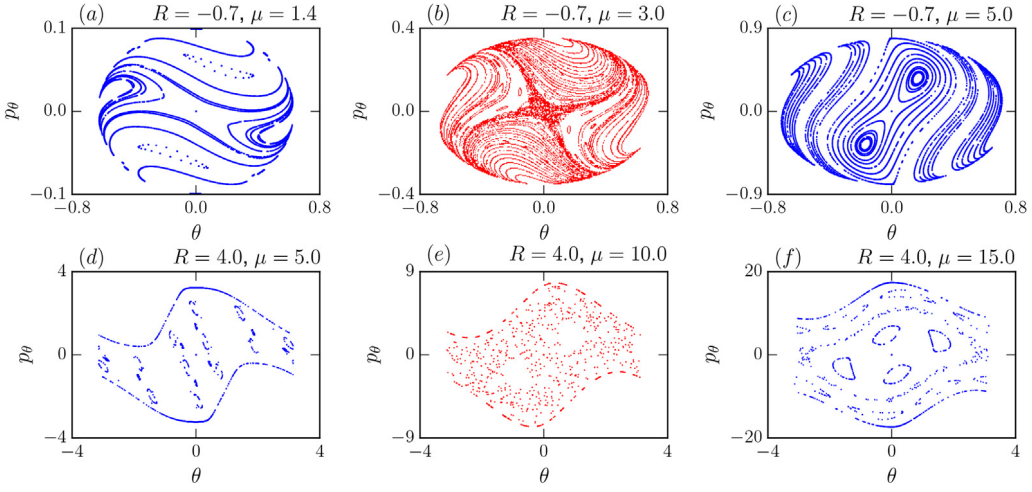

Fig. 2. *Order-chaos-order transition in the PEP.* Subplots (a), (b), and (c), i.e., the upper row, depict the Poincaré sections in θ-p_θ plane for $\mu = 1.4$, 3, and 5 respectively in the libration regime ($R = -0.7$). Similarly, subplots (d), (e), and (f), i.e., the lower row, showcase the Poincaré sections for $\mu = 5$, 10, and 15 respectively in the rotation regime ($R = 4.0$). The blue plots indicate the predominantly regular state whereas the red plots highlight the widespread chaos. To construct each Poincaré section, we have solved the equations of motion of the PEP numerically for various initial conditions at fixed value of R and μ and then taken the section of trajectories in $\theta - p_\theta$ plane for fixed $\delta r = 0$ and $p_r > 0$. (For interpretation of the references to colour in this figure legend, the reader is referred to the web version of this article.)

In order to facilitate analytical investigation of the order-chaos-order phenomenon in the PEP, we choose to work in the small amplitude limit for the motion of the PEP. Although this effectively restricts us to remain within the libration regime of the PEP, still even within this limit finding the quantitative mechanism for the order-chaos-order phenomenon remains a challenging problem whose answer happens to be quite nontrivial as we show in this paper. To begin with, however, we have to decide on the approximated Hamiltonian of the PEP so that it can be perturbatively tackled for the problem in hand.

2. The PEP and the Chirikov overlap criterion

The Hamiltonian of the PEP in the Cartesian coordinate system is [10,19]

$$H = \frac{1}{2m}({p_x}^2 + {p_z}^2) - mgz + \frac{1}{2}k_s(\sqrt{x^2 + (l-z)^2} - l_0)^2. \tag{2}$$

Here, x and z respectively are the horizontal and the vertical components of the displacement of the mass from the equilibrium point, and p_x and p_z are the corresponding conjugate momenta. Also, $l = l_0 + mg/k_s$. Since the full Hamiltonian (Eq. (2)) is not analytically tractable, we need an appropriately approximated version of the Hamiltonian. It can be argued (see Appendix A) that in order to be able to see chaos in the system, the Hamiltonian should be approximated such that at least the terms up to the fourth order are retained, i.e.,

$$H = \frac{1}{2m}({p_x}^2 + {p_z}^2) + \frac{1}{2}m\omega_{10}^2x^2 + \frac{1}{2}m\omega_{20}^2z^2 + m\nu_1x^2z + \frac{1}{4}m\nu_2x^4 - m\nu_2x^2z^2\,, \tag{3}$$

where $\omega_{10}^2 \equiv (k_s/m)(1 - (l_0/l)) = g/l$, $\omega_{20}^2 \equiv k_s/m$, $\nu_1 \equiv (k_s/2m)(l_0/l^2) = (\omega_{20}^2 - \omega_{10}^2)/2l$, and $\nu_2 \equiv (k_s/2m)(l_0/l^3) = (\omega_{20}^2 - \omega_{10}^2)/2l^2$.

We treat the PEP as if it is a nonlinearly coupled one-degree-of-freedom pendulum system and a one-degree-of-freedom Hookian spring system. In the absence of this coupling, the PEP is thus an integrable system that incidentally is an iso-energetically non-degenerate although not a non-degenerate KAM system [24,32]. The coupling makes the system nonintegrable but in the limit of small amplitude oscillations (librations) – as we consider in this paper – the PEP is a nearly integrable system that comes under the purview of KAM theory, and hence can also possibly be tackled by the Chirikov's method of resonance overlap. With this in mind, we first go on to write the optimally truncated Hamiltonian in terms of the action–angle variables of the unperturbed Hamiltonian (zero aforementioned coupling) as discussed below.

2.1. Resonances in the PEP

Assuming that the extension in the length of the spring in motion is much smaller than the rest length of the spring (i.e., $\delta r \ll l_0$), the Hamiltonian given by Eq. (1) – up to the fourth-order terms – can be cast as follows:

$$H(\delta r, \theta, p_r, p_\theta) = H_p^0(\theta, p_\theta) + H_s^0(\delta r, p_r) + H_{\text{pert}}(\delta r, \theta, p_r, p_\theta) + E_{\min}, \tag{4}$$

where,

$$H_p^0 \equiv \frac{p_\theta^2}{2ml^2} + mgl(1 - \cos\theta), \tag{5a}$$

$$H_s^0 \equiv \frac{p_r^2}{2m} + \frac{1}{2}k_s\delta r^2, \tag{5b}$$

$$H_{\text{pert}} \equiv \frac{p_\theta^2}{2ml^2}\left(-\frac{2\delta r}{l} + \frac{3\delta r^2}{l^2}\right) + mg\delta r(1 - \cos\theta)\,. \tag{5c}$$

If the action–angle variables for H_p^0 be denoted by (J_p^0, ϕ_p^0) and that for H_s^0 be denoted by (J_s^0, ϕ_s^0), then in the libration regime one concludes [24,32]:

$$J_p^0 = \frac{8ml^2\omega_p^0}{\pi}\left(E(k) - (1-k^2)K(k)\right)\,, \tag{6a}$$

$$\phi_p^0 = \frac{\pi}{2K(k)}F\left(\frac{1}{k}\sin\frac{\theta}{2}; k\right)\,, \tag{6b}$$

$$J_s^0 = \frac{H_s^0}{\Omega_s^0}\,, \tag{6c}$$

$$\phi_s^0 = \sin^{-1}\left(\sqrt{\frac{m\omega_s^0}{2J_s^0}}\delta r\right)\,, \tag{6d}$$

where $k^2 \equiv H_p^0/2mgl$, $\Omega_s^0 \equiv \omega_s^0 = \sqrt{k_s/m}$, $K(k)$ is the complete elliptic integral of first kind, $E(k)$ is the complete elliptic integral of second kind, and $F(k)$ is incomplete elliptic integral of the first kind [33]. The frequency, $\Omega_p^0(k)$, corresponding to the unperturbed pendulum is given by: $\Omega_p^0(k) = \pi\omega_p^0/2K(k)$.

Furthermore, the equation of motion corresponding to the unperturbed simple pendulum yields [24,32],

$$\theta = 2\arcsin\left[k\,\mathrm{sn}\left(\frac{2}{\pi}K(k)\phi_p^0, k\right)\right]\,, \tag{7a}$$

$$p_\theta = 2ml\sqrt{gl}k\,\mathrm{cn}\left(\frac{2}{\pi}K(k)\phi_p^0, k\right)\,. \tag{7b}$$

On using Eq. (6d), Eq. (7a), and Eq. (7b); and the series expansions [34] for sn^2 and cn^2 in Eq. (5c), we get the following expression for H_{pert} in terms of the action–angle variables of the unperturbed system:

$$\begin{aligned}
H_{\text{pert}} = {} & -4mgA_s\frac{E(k) - k'^2K(k)}{K(k)}\sin\phi_s^0 \\
& + \frac{6mgA_s^2}{l}\frac{E(k) - k'^2K(k)}{K(k)}\sin^2\phi_s^0 \\
& + \frac{\pi^2}{K(k)^2}\frac{6mgA_s^2}{l}\sum_{n=1}^{\infty}C_n\cos 2n\phi_p^0 \\
& + 2mgA_s\frac{K(k) - E(k)}{K(k)}\sin\phi_s^0 \\
& + \frac{\pi^2}{K(k)^2}6mgA_s\sum_{n=1}^{\infty}C_n\left[\sin(2n\phi_p^0 - \phi_s^0) - \sin(2n\phi_p^0 + \phi_s^0)\right] \\
& - \frac{\pi^2}{K(k)^2}\frac{3mgA_s^2}{l}\sum_{n=1}^{\infty}C_n\left[\cos(2n\phi_p^0 - 2\phi_s^0)\right. \\
& \left. + \cos(2n\phi_p^0 + 2\phi_s^0)\right].
\end{aligned} \tag{8}$$

Here, $A_s \equiv \sqrt{2J_s^0/m\omega_s^0}$ and $C_n \equiv nq^n/(1 - q^{2n})$ with $q \equiv \exp(-\pi K(\sqrt{1-k^2})/K(k))$. The resonance terms explicitly present in the Hamiltonian are called the primary resonances [24,35,36], e.g., the $2n : 1$ and the $2n : 2$ resonances present in Eq. (8) are the primary resonances whose strengths (Fourier coefficients) respectively are

$$V_{2n,1} = 6mgC_n\sqrt{\frac{2J_s^0}{m\omega_s^0}}\frac{\pi^2}{K(k)^2}\,, \tag{9a}$$

$$V_{2n,2} = -C_n\frac{3mg}{l}\frac{2J_s^0}{m\omega_s^0}\frac{\pi^2}{K(k)^2}\,. \tag{9b}$$

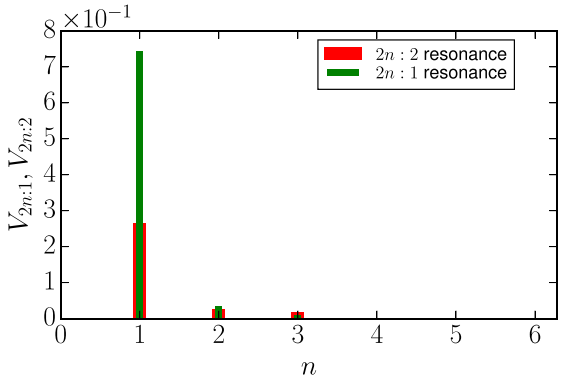

Fig. 3. *The* 2 : 1 *primary resonance is the strongest.* This plot compares the strengths of the most dominating primary resonances as given by Eq. (9). The thinner green bars and the thicker red bars respectively correspond to the resonances of type $2n:1$ and $2n:2$.

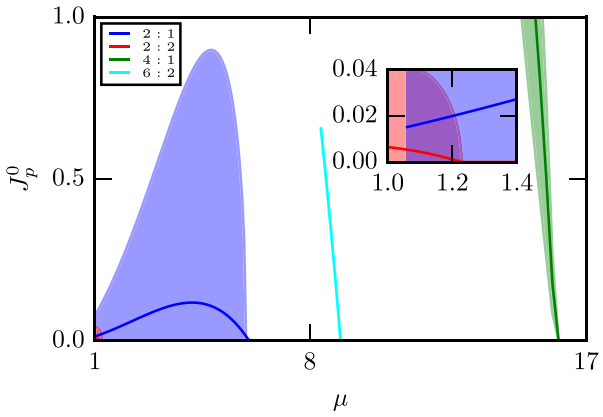

Fig. 4. *No overlap of the dominant primary resonances in the libration regime.* The solid curves represent the values of action J_p^0 of the resonance centres for $R = -0.7$ as μ is varied. The blue, the red, the green, and the cyan curves respectively correspond to the 2 : 1, the 2 : 2, the 4 : 1, and the 6 : 2 primary resonances. The width of each resonance is shown by the shaded region sandwiching the corresponding solid curve; the lighter colours of the shaded regions have been chosen to match with the corresponding darker colour of the solid curve. The width is relatively too small to be seen around the cyan line. The overlap (purple region) between the 2 : 1 and the 2 : 2 resonances, as seen in the inset, is spurious (see text).

As we note in Fig. 3, the strengths of the resonances decrease rapidly with the increasing value of n; among all the resonances, the 2 : 1 resonance is the most dominating one.

For later discussion, we remark here that it is well known that in case there was a single resonance term present in the Hamiltonian, one could introduce a set of new action–angle variables such that the Hamiltonian becomes integrable, i.e., a function of the new action alone. If now more primary resonances (in terms of the old action–angle variable) are added to the Hamiltonian, then the resonance terms – cast in terms of the aforementioned new action–angle variables – give rise to the so-called secondary resonances [24,35,36].

2.2. Resonances' positions and widths

For the unperturbed Hamiltonian, an $n_p : n_s$ resonance – n_p and n_s being nonzero integers – occurs when, $(n_p\omega_p^0 - n_s\omega_s^0) = 0$. Here, $\omega_p^0 = \dot{\phi}_p^0$ and $\omega_s^0 = \dot{\phi}_s^0$ are the frequencies corresponding to the unperturbed Hamiltonian. To understand the implication of the resonance, one may recall the textbook case of a sinusoidally forced simple harmonic oscillator,

$$\ddot{x} + \Omega^2 x = \cos \Omega_{\rm ext} t, \tag{10}$$

that at $\Omega_{\rm ext} = \Omega$ (i.e., when the frequency of the external forcing is equal to the natural frequency of the oscillator) is said to be at resonance condition. The particular integral of Eq. (10) is $t \sin \Omega_{\rm ext} t/2\Omega_{\rm ext}$ and not $\cos \Omega_{\rm ext} t/(\Omega^2 - \Omega_{\rm ext}^2)$ that is valid only when $\Omega_{\rm ext} \neq \Omega$. Hence, we note that the appearance of the aperiodic solution is equivalent to the denominator, $\Omega^2 - \Omega_{\rm ext}^2$, being zero at resonance. Analogously, in the case of the PEP, the resonance condition brings forth the infamous problem of the small denominators, and thus, prevents the solution from being periodic in $\phi_s^{(0)}$ and $\phi_p^{(0)}$. For the perturbed Hamiltonian, $\dot{\phi}_p^0$ and $\dot{\phi}_s^0$ that represent the frequencies of the system is not ω_p^0 and ω_s^0 respectively; therefore, the resonance condition for the perturbed Hamiltonian is better expressed in terms of the time derivatives of the angle variables rather than the frequencies of the unperturbed Hamiltonian, i.e.,

$$n_p\dot{\phi}_p^0 - n_s\dot{\phi}_s^0 = 0\,. \tag{11}$$

We now intend to locate the position of the resonances in the phase space. The approximate location can be found out in a rather straightforward manner if one considers every resonance in isolation, meaning, if we want to find the location of the 2 : 1 resonance, we work with the following truncated Hamiltonian:

$$H = J_s^0\omega_s^0 + 2(mgk)^2\frac{\mu}{k_s} + 6mg\frac{q}{1-q^2}\sqrt{\frac{2J_s^0}{m\omega_s^0}} \times \frac{\pi^2}{K(k)^2}\sin(2\phi_p^0 - \phi_s^0) + E_{\rm min}\,. \tag{12}$$

This approximation, in effect, is equivalent to working with the averaged dynamics about the resonance in hand so that the rest of the resonant and the non-resonant terms appear to be relatively highly oscillating, and consequently, their effect over a complete period is negligible. We may remark here that the $|n_p| : -|n_s|$ resonances are not realized in our system because they do not satisfy Eq. (11) for the strictly positive values of $\dot{\phi}_p^0$ and $\dot{\phi}_s^0$ as is the case for the system in hand.

We now perform a canonical transformation via the type-2 generating function, $S_2 = \frac{1}{2}\phi_s^0(I_1 - I_2) + \phi_p^0 I_2$, to go from the old coordinates, $(\phi_s^0, \phi_p^0, J_s^0, J_p^0)$, to the new coordinates, $(\psi_1, \psi_2, I_1, I_2)$. The explicit transformations between these coordinates are: $\psi_1 = \phi_s^0/2$, $\psi_2 = \phi_p^0 - \phi_s^0/2$, $J_s^0 = (I_1 - I_2)/2$, and $J_p^0 = I_2$. It should be noted from Eq. (11) that the transformation is such that the condition for the 2 : 1 resonance reduces to $\dot{\psi}_2 = 0$. Consequently, the fixed points – given by $\dot{I}_1 = \dot{I}_2 = \dot{\psi}_2 = 0$ – of the Poincaré map describing the dynamics on the points of intersections of the phase trajectories with the hypersurface, $\psi_1 =$ constant, locates the 2 : 1 resonance on the corresponding I_1-I_2-ψ_2 hypersurface. At the fixed point, thus, $\psi_2 = (2j+1)\pi/4$ (mod 2π), where $j \in \{0, 1, 2, \ldots\}$. Specifically, in θ-p_θ plane, where $\phi_s^0 = 0$, the 2 : 1 resonance is located at $\phi_p^0 = (2j+1)\pi/4$. The fixed points corresponding to $j = 0$ and $j = 2$ are the two centres of the 2 : 1 resonance. This can be ascertained [29] by the fact that at these points, $(d\Omega_p^0/dJ_p^0)V_{2,1}\sin(2\phi_p^0 - \phi_s^0) < 0$. Likewise, the fixed points corresponding to $j = 1$ and $j = 3$—for which $(d\Omega_p^0/dJ_p^0)V_{2,1}\sin(2\phi_p^0 - \phi_s^0) > 0$—are the saddle points of the 2 : 1 resonance.

Subsequently, the values of the actions J_s^0 and J_p^0 at the resonance centre can be calculated using Eqs. (11) and (12). In Fig. 4, we show the value of the action variable J_p^0 of the 2 : 1 resonance for fixed $R = -0.7$ (libration regime) and varying μ. We note that the *primary* 2 : 1 resonance appears at $\mu = 1$ and vanishes around $\mu = 6$. In the similar fashion we can find J_p^0 vs. μ for any

other primary resonances, e.g., 2 : 2, 4 : 1, and 6 : 2 resonances as depicted in Fig. 4.

Under the same setting of isolated resonance as discussed above, the resonance half-width of any $n_p : n_s$ resonance is given by the following expression [37]:

$$\frac{1}{2}(\Delta J_p^0)_{n_p,n_s} = 2\sqrt{\frac{|V_{n_p,n_s}|}{d\Omega_p^0/dJ_p^0}}. \tag{13}$$

For the PEP, therefore, the half-widths of the $2n : 1$ and the $2n : 2$ resonances can be calculated to be:

$$\frac{1}{2}(\Delta J_p^0)_{2n,1} = 2\sqrt{96m^2gA_sl^2C_n\frac{k^2(1-k^2)K(k)}{E(k)-(1-k^2)K(k)}}, \tag{14a}$$

$$\frac{1}{2}(\Delta J_p^0)_{2n,2} = 2\sqrt{48m^2gA_s^2lC_n\frac{k^2(1-k^2)K(k)}{E(k)-(1-k^2)K(k)}}. \tag{14b}$$

Fig. 4 also exhibits the half-widths for some of the primary resonances, viz., 2 : 1, 2 : 2, 4 : 1, and 6 : 2. The 2 : 1 resonance has the maximum width, and the width of the higher resonances are negligibly small. As a result, apart from an almost unnoticeable overlap between the 2 : 1 and the 2 : 2 resonances for approximately $\mu \in (1.1, 1.2)$, there is no overlap between the primary resonances. We emphasize that we have actually overestimated the widths. It is evident from Fig. 4 that $(\Delta J_p^0)_{2,1}$ is, in fact, greater than J_p^0 of the 2 : 1 resonance and this fact is not in line with the premise of the Chirikov method. Same is the case with the 2 : 2 resonance. Hence, the overlap between the 2 : 1 and the 2 : 2 resonances, as seen in the inset of Fig. 4, is spurious. Probably, other methods of finding widespread chaos, e.g., Greene's method [38], could be more accurate.

3. Origin of the order-chaos-order transition

In view of the discussion in the preceding section, it is quite intriguing that the widespread chaos, and hence the order-chaos-order transition, should appear in the PEP; at least, the Chirikov resonance overlap criterion as employed on the primary resonances seems to rule out any such transition. However, there is no denying that the order-chaos-order transition does happen in the PEP. Hence, it is logical to conjecture that the chaos in the transition might owe its origin to the secondary resonances.

In principle, the secondary resonances can be identified using the Birkhoff normalization technique [36] that is performed near a particular resonance, say $n_p^0\omega_p^0 - n_s^0\omega_s^0 = 0$, with a view to eliminate the other resonances. The resulting new transformed Hamiltonian is, in general, an infinite series of new resonant terms which correspond to the secondary resonances. (It may happen that some of the new resonant terms are similar to the primary resonances.) The Birkhoff normalization technique can be repeatedly applied to arbitrary order so that further resonances like tertiary resonances are generated. However, the PEP is not a simple enough system to facilitate the analytical search of the secondary and the further resonances via the normalization technique. Hence, we resort to systematic numerical experiments to find the secondary resonances and hence to pinpoint the origin of the order-chaos-order in the PEP.

3.1. Results for the truncated Hamiltonian of the PEP

Recall that in Section 2, we have concerned ourselves with the approximated Hamiltonian so that we can analytically pinpoint the locations of the resonances and find the strengths of the resonances. Therefore, when in this section, we turn to the numerical simulations, we still keep using the approximated Hamiltonian so that the correctness of the numerical results can be ascertained using the aforementioned analytically obtained results. We do understand that using the full Hamiltonian is technically more accurate. In that case, however, the numerically obtained positions of the resonances would not follow the analytical predictions (obtained using the approximated Hamiltonian) closely; but the trend is expected to remain qualitatively similar. Specifically, the lower order primary resonances should be robust to our choice of Hamiltonian (approximated or full) owing to their large strengths. For example, as we note later in this paper, the primary resonances 2:1 and 4:1 appear clearly at the same values of μ for both the approximated Hamiltonian and the full Hamiltonian. In view of these facts, in this section we numerically time-evolve the PEP using the approximated Hamiltonian given in Eq. (4) and plot the Poincaré sections in Fig. 5. A similar study with the full Hamiltonian is done subsequently.

To construct each Poincaré section, we solve the corresponding equations of motion of the PEP using various initial conditions at the fixed values of $R\ (= -0.7)$ and μ, and take the section of trajectories in θ-p_θ plane while fixing $\delta r = 0$ and $p_r > 0$. The very first thing we observe is that our analytical calculations – summarized in Fig. 4 – are validated by the plots in Fig. 5: (i) the 2 : 2 and the 2 : 1 primary resonances start at $\mu = 1^+$, (ii) the 2 : 2 resonance disappears at around $\mu \approx 1.2$, (iii) the 2 : 1 primary resonance vanishes at $\mu \approx 6$, (iv) around $\mu \approx 8.0$, we see the emergence of the 6 : 2 primary resonance which disappears at around $\mu \approx 9$, and (v) at $\mu \approx 14.0$, we see the 4 : 1 primary resonance appear.

Coming to the main point of this paper, we observe that the order-chaos-order phenomenon is distinctly visible in the plots. In fact, as we have conjectured earlier in the paper, this phenomenon owes its origin to the presence of the resonances that are not explicitly present in the perturbative part of the Hamiltonian (see Eq. (8)) under consideration. In Fig. 5, we notice that starting from $\mu \approx 1.43$ there is a series of secondary resonances, viz., 6 : 5, 5 : 4, 4 : 3, 6 : 4, and 2 : 1, that appear with increasing μ. For the problem in hand, the most crucial secondary resonance is the 2 : 1 secondary resonance that arises at $\mu \approx 2.7$. At $\mu \approx 3.0$, there is *an overlap of the* 2 : 1 *primary resonance and the* 2 : 1 *secondary resonance* which brings forth the widespread chaos needed for the initiation of the order-chaos-order phenomenon. As mentioned earlier, at around $\mu \approx 6$, the 2 : 1 primary resonance vanishes but the 2 : 1 secondary resonance is still existent although with a decreased width. There is no further discernible overlap between the resonances beyond $\mu = 6$, or in other words, the order has been reestablished in the system.

Since the chaos in the system is most strongly observed in the vicinity of $\mu = 4$, a close investigation of the overlap of the primary and the secondary 2 : 1 resonances near autoparametric resonance condition is insightful. In Fig. 6, we plot the Poincaré sections for the values of μ ranging from 3.3 to 4.7, and note that the order-chaos-order sequence is accompanied by the reconnection between the saddle of one 2 : 1 resonance and the two pairs of centre points of the other 2 : 1 resonance. Specifically, in this range, for $\mu < 4$, $(0, 0)$ is the saddle of the secondary 2 : 1 resonance (see Figs. 6(a)–6(h)). The size of this resonance increases with μ, and at $\mu = 4$, the separatrix of the secondary resonance covers a large portion of the phase space and consequently overlaps with the primary 2 : 1 resonance bringing forth the widespread chaos. For $\mu > 4.0$, a reconnection takes place and $(0, 0)$ becomes the saddle of the primary 2 : 1 resonance (see Figs. 6(i)–6(o)). This reconnection phenomenon in the order-chaos-order transition not only known for the PEP [10,39] but also in another closely related system – spring–mass–pendulum system – showing similar 2 : 1 autoparametric resonance [40].

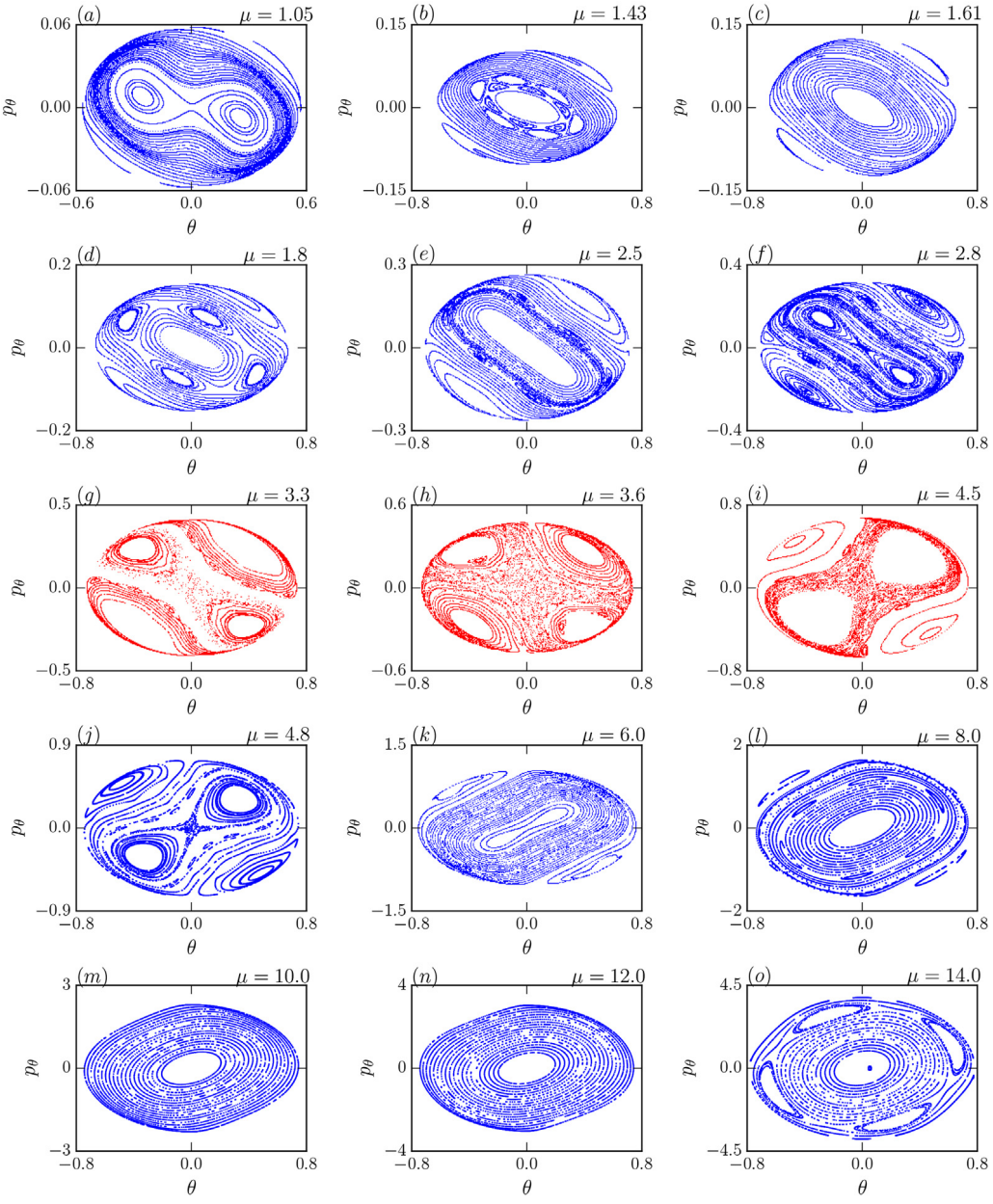

Fig. 5. *Order-chaos-order transition in the PEP approximated by Eq. (4).* This figure represents the Poincaré sections at $R = -0.7$ for different values of μ in θ-p_θ plane. The blue plots indicate the predominantly regular states whereas the red plots highlight the widespread chaos. We note the presence of the 2 : 1 (subplots (a)–(k)) and the 2 : 2 (subplot (a)) primary resonances for smaller values of μ. Before the transition to the chaotic state various secondary resonances, e.g., 6 : 5 (in subplot (b)), 5 : 4 (in subplot (c)), 4 : 3 (in subplot (d)), 6 : 4 (in subplot (e)) and 2 : 1 (in subplot (f)) are observed between $\mu = 1^+$ to $\mu \approx 2.8$. The transition from the ordered states (subplots (a)–(f)) to the chaotic states (subplots (g)–(i)) starts at $\mu \approx 3.0$ due to the overlap between the 2 : 1 primary and the 2 : 1 secondary resonances. The widths of the resonances decrease with further increase in μ leading to another transition from the chaotic state to the ordered state at $\mu \approx 4.8$. At $\mu \approx 6.0$, the 2 : 1 primary resonance vanishes (subplot (k)). Other primary resonances, viz., the 6 : 2 (subplot (l)) and the 4 : 1 (subplot (o)) are also observed but there is no resonance overlap and the system stays mostly in the ordered states (subplots (j)–(o)). (For interpretation of the references to colour in this figure legend, the reader is referred to the web version of this article.)

3.2. Results for the full Hamiltonian of the PEP

Having used a combination of numerical and analytical methods to unravel the mechanism of the order-chaos-order transition in the approximated Hamiltonian of the PEP, we must find out how robust the results are if the full Hamiltonian of the PEP is considered. We now show that the order-chaos-order transition, via the reconnection between the saddle of one 2 : 1 resonance and the two pairs of centre points of the other 2 : 1 resonance, is a robust phenomenon; i.e., the mechanism of the transition remains qualitatively unchanged even if an infinite number of nonlinear terms beyond quartic order are ignored in the Hamiltonian of the PEP.

To this end, we present Fig. 7 containing the Poincaré sections corresponding to the PEP Hamiltonian (Eq. (1)) for various values of μ and $R = -0.7$. We see that the qualitative picture is similar to what is obtained in Fig. 5 using the approximated Hamiltonian of the PEP. Specifically, the locations, the strengths, and the dependence on μ of the lower order primary resonances, e.g., 2 : 1 and 4 : 1 remain almost unaltered. As far as the higher order resonances appearing in the approximated Hamiltonian are concerned, they exist even in the case of the full Hamiltonian but

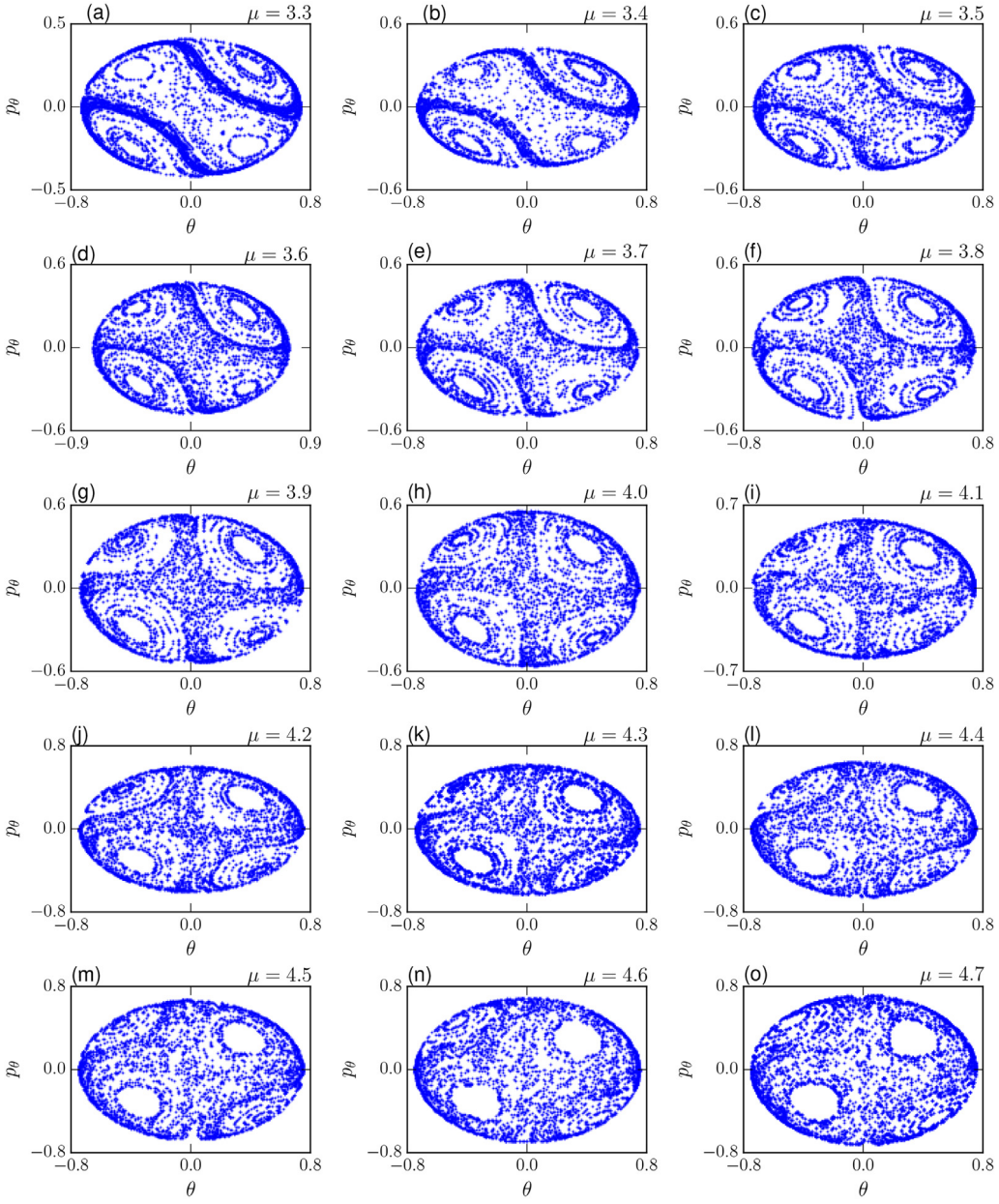

Fig. 6. *Reconnection in the primary* 2 : 1 *and the secondary* 2 : 1 *resonances near* $\mu = 4.0$ *using the approximated Hamiltonian (Eq. (4)).* This figure depicts the Poincaré sections in θ-p_θ plane for $\mu = 3.3$ to 4.7 at $R = -0.7$. For $\mu < 4.0$, $(\theta, p_\theta) = (0, 0)$ is the saddle point corresponding to the secondary 2 : 1 resonance; and for $\mu > 4.0$, $(\theta, p_\theta) = (0, 0)$ is the saddle point corresponding to the primary 2 : 1 resonance.

their strengths and the values of the μ at which they appear may slightly differ.

Similar to the Poincaré sections (Figs. 5(g)–5(i)) of the approximated PEP, here also we observe that the chaos is dominant around $\mu = 4.0$ due to the overlap of the primary and the secondary 2 : 1 resonances (Figs. 7(d)–7(f)). Additionally, we observe in Fig. 8 that the order-chaos-order is mediated through the reconnection between the saddle of one 2 : 1 resonance and the two pairs of centre points of the other 2 : 1 resonance. We also observe the secondary 4 : 3 (Fig. 7(a)) and 6 : 4 (Fig. 7(b)) resonances in the Poincaré sections at $\mu = 1.8$ and 2.5 respectively. The secondary 2 : 1 resonance (Fig. 7(c)) emerges at $\mu \approx 2.8$. While the primary 2 : 1 resonance vanishes beyond $\mu \approx 6.0$, the secondary 2 : 1 resonance still exists. Similar to the approximated case, no resonance overlap is observed beyond $\mu \approx 6.0$ and the system acquires the dominantly regular state again. The 6 : 2 primary resonance appears at $\mu \approx 6.8$ which also arises in the approximated Hamiltonian case but for slightly higher value of $\mu \approx 8.0$. At $\mu \approx 14.0$, we find the primary 4 : 1 resonance which also matches with our analytical prediction in Fig. 4 and also with the Poincaré section (Fig. 5(o)) for approximated Hamiltonian.

The spread of chaos at certain values of μ, as seen in Fig. 7, can be extended if R is increased. This can be concluded if we compare the plots for $R = -0.7$ with corresponding plot of the Poincaré sections at $R = -0.3$, i.e., for relatively higher value of energy (Fig. 9). Although the strengths of the primary and the secondary resonances change, they all appear in the case of $R = -0.3$ as well. Consequently, the order-chaos-order transition is observed as well. It may be worth pointing out that unlike the case of some other similar systems exhibiting order-chaos-order sequence (e.g., two-degree-of-freedom-spring–mass–pendulum system [40]), varying either the ratio of the spring and the pendulum frequencies or the total system energy leads to an order-chaos-order sequence in the PEP [10].

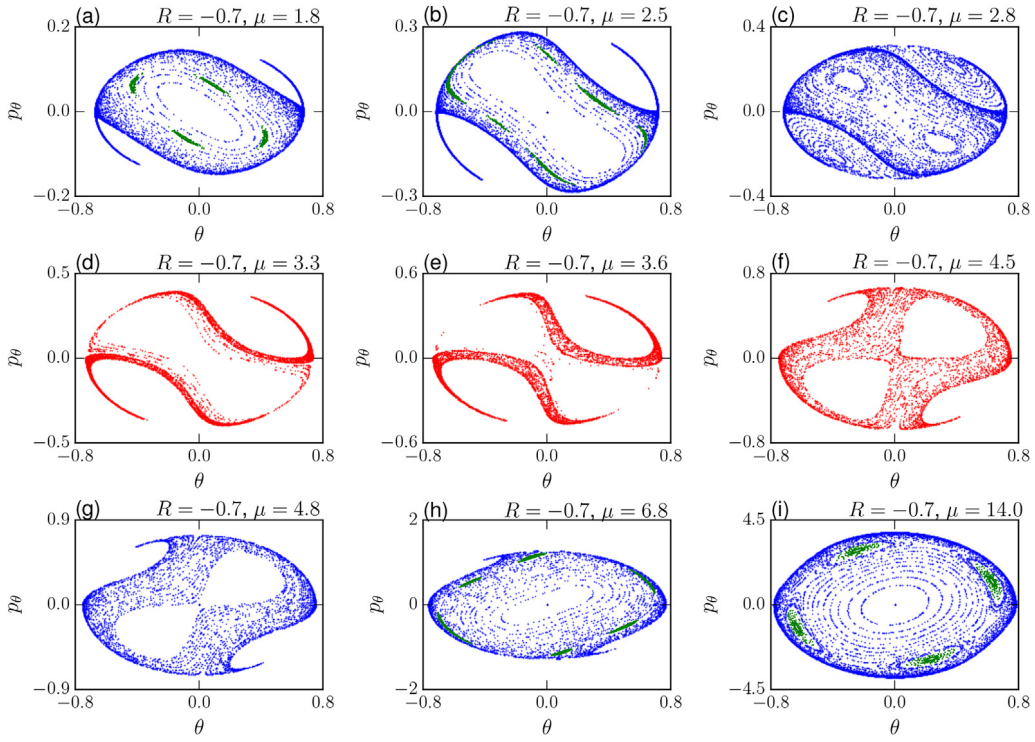

Fig. 7. *Order-chaos-order transition in the PEP at $R = -0.7$ using Eq. (1).* The blue colour indicates the predominantly regular states, green colour is used to highlight some small resonance islands, and the red colour indicates the widespread chaos. We note the presence of the primary 2 : 1 resonance (subplots (a)–(h)) for $\mu \in (1^+, 6.8)$. Before the transition to the chaotic state various secondary resonances, e.g., 4 : 3 (in subplot (a)), 6 : 4 (in subplot (b)) and 2 : 1 (in subplot (c)) first appear between $\mu = 1^+$ to $\mu \approx 2.8$. The transition from the ordered states (subplots (a)–(c)) to the chaotic states (subplots (d)–(f)) starts at $\mu \approx 3.3$ due to the overlap between the 2 : 1 primary and the 2 : 1 secondary resonances. Other primary resonances, viz., 6 : 2 (subplot (h)) and 4 : 1 (subplot (i)) are also observed but there is no resonance overlap and the system stays mostly in the ordered states (subplots (g)–(i)). (For interpretation of the references to colour in this figure legend, the reader is referred to the web version of this article.)

Recall that in θ-p_θ plots, following reconnection at $\mu = 4$, $(0, 0)$—that is the saddle of the secondary 2 : 1 resonance for $2.8 \lesssim \mu \lesssim 4.0$—becomes the saddle of the primary 2 : 1 resonance for $\mu > 4.0$. There is chaos about the separatrix. In the neighbourhood of the autoparametric resonance condition, the spring mode excites the oscillation along horizontal direction, i.e., the saddle structure grows (initiating the chaos in the system) and for the other values of μ further away from $\mu \approx 4$, the saddle structure remains close to the origin (system remains predominantly regular) [10]. Similarly, the swing mode also excites the oscillation along vertical direction for $\mu \approx 4.0$. Thus, the energy in the PEP is continuously exchanged between the spring and the swing modes. This exchange of energy has been studied in detail [39]. It is seen that at $\mu = 4.0$, the region of widespread chaos in the PEP increases as the energy of the system increases leading to an interesting fact which is best understood if we treat the PEP as a nonlinearly coupled system of a one-degree-of-freedom pendulum and a one-degree-of-freedom Hookian spring. We can, thus, split the energy content of the PEP in three parts: energy in the pendulum, energy in the spring, and energy in the nonlinear coupling. At the autoparametric resonance condition, when only the spring or the pendulum moves, all three parts of the energy remain constant in time but when the spring mode and the swing mode exchange energy, the coupling energy does small oscillations and paves the way for the energy transfer between the two modes. In contrast, when the PEP is driven away from the autoparametric resonance condition, say, by increasing the initial energy of the system, many disconnected resonance islands are created in the phase space such that all the three parts of the energy terms oscillate regularly and energy is regularly exchanged between the two modes—a signature of quasiperiodic motion.

3.3. Trajectories in the physical x-z space

In order to get the more insight into the fundamentally different kinds of dynamics of the PEP in the physical space and how these correlate to our understanding of the phase space of the PEP, we also plot the trajectories made by the point mass of the PEP in the physical x-z space. In Fig. 10, we present some illustrative plots of the trajectories for the chaotic and the quasiperiodic motions in the x-z plane. In the plots, μ ranges from 3.8 to 4.2 and $R = -0.7$. To be able to distinguish the chaotic and the quasiperiodic motions qualitatively in the physical space, we evolve the system for two nearby initial conditions in θ-p_θ plane ($\delta r = 0.0$) for a sufficiently long time. As an aside, it may be noted that the value of p_r can be calculated using the Hamiltonian of the PEP since energy is conserved for each trajectory.

In the first column of the figure (Figs. 10(a)–10(e)), we take two nearby initial conditions – $(0.01, 0.01)$ and $(0.011, 0.01)$ – near the separatrix, where chaos is supposed to have set in. In the second column (Figs. 10(f)–10(j)) and the third column (Figs. 10(k)–10(o)) of the figure, we respectively take the initial conditions near the primary and the secondary 2 : 1 resonances inside which the motions are supposed to be quasiperiodic: for the primary resonance the initial conditions are $(0.4, 0.4)$ and $(0.401, 0.4)$; whereas the initial conditions, $(-0.4, 0.4)$ and $(-0.401, 0.4)$), are used for the secondary resonance. We observe that the two nearby trajectories in the case of the chaotic motion do not always remain close to each other when they are evolved for a sufficiently long time, whereas the nearby trajectories always move close to each other in the case of the quasiperiodic motions. In order to quantitatively distinguish these two types of motion, we also calculate the maximum Lyapunov exponent for the trajectories, and as expected, the exponent is positive

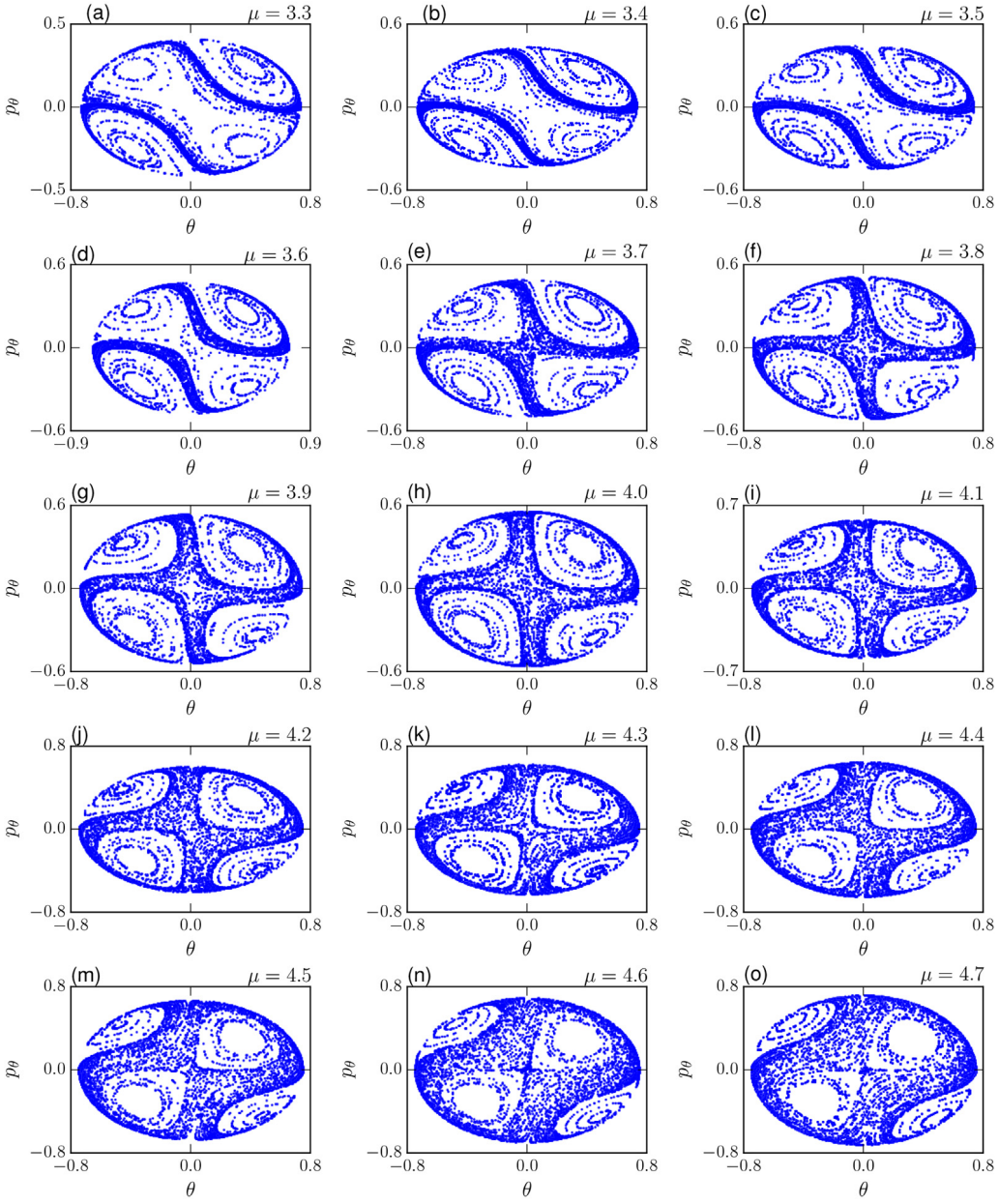

Fig. 8. *Reconnection in the primary* 2 : 1 *and the secondary* 2 : 1 *resonances near* $\mu = 4.0$ *using Eq.* (1). This plot depicts the Poincaré sections in θ-p_θ plane for $\mu = 3.3$ to 4.7 at $R = -0.7$. For $\mu < 4.0$, $(\theta, p_\theta) = (0, 0)$ is the saddle point corresponding to the secondary 2 : 1 resonance; and for $\mu > 4.0$, $(\theta, p_\theta) = (0, 0)$ is the saddle point corresponding to the primary 2 : 1 resonance.

definite and zero (approximately) for the chaotic trajectories and the quasiperiodic trajectories respectively.

A very perceptible change in the range of the motion of the point mass along z-direction with increasing μ may be noted for the cases of the quasiperiodic motions; e.g., the second column of Fig. 10 that corresponds to the primary 2 : 1 resonance, depicts a monotonous decrease in the range with increasing μ. The effect is most clearly seen at $x = 0$. Since $x = 0$ corresponds to $\theta = 0$ (recall that $x = (l + \delta r)\sin\theta$), the reason behind this observation is best understood with the help of the Poincaré sections in δr-p_r plane ($\theta = 0.0$). In Fig. 11(a), we present a plot consisting of such Poincaré sections for the initial conditions corresponding to the five blue trajectories present in the second column of Fig. 10. We observe that with increasing μ, the torus on which the fixed initial condition is chosen shrinks in size with increasing μ such that the maximum value of δr for the torus decreases. Thus, it straightforwardly follows that range of the motion along z-direction should decrease (recall that $z = -(l + \delta r)\cos\theta$.). Also, since the shrinkage in the torus's size is not accompanied by an appreciable change in the minimum value of δr, the decrease in the width of the region covered by the trajectory corresponding to the primary 2 : 1 resonance (see Figs. 10(f)–10(j)) is dominantly from the upper side.

The change in the range of the motion along z-direction with increasing μ for the case of the secondary 2 : 1 resonance can be similarly explained using Fig. 11(b) that exhibits the Poincaré sections in δr-p_r plane ($\theta = 0.0$) for the initial conditions corresponding to the five blue trajectories present in the third column of Fig. 10. However, when compared with the case of the primary 2 : 1 resonance, this case is different in at least two aspects: Firstly, the range monotonously decreases with increasing μ for $\mu \leq 4$ in the neighbourhood of $\mu = 4$ (see Figs. 10(k)–10(m)) and it monotonously increases for $\mu > 4$ in the neighbourhood of $\mu = 4$ (see Figs. 10(n)–10(o)). Secondly, the shrinkage in the size

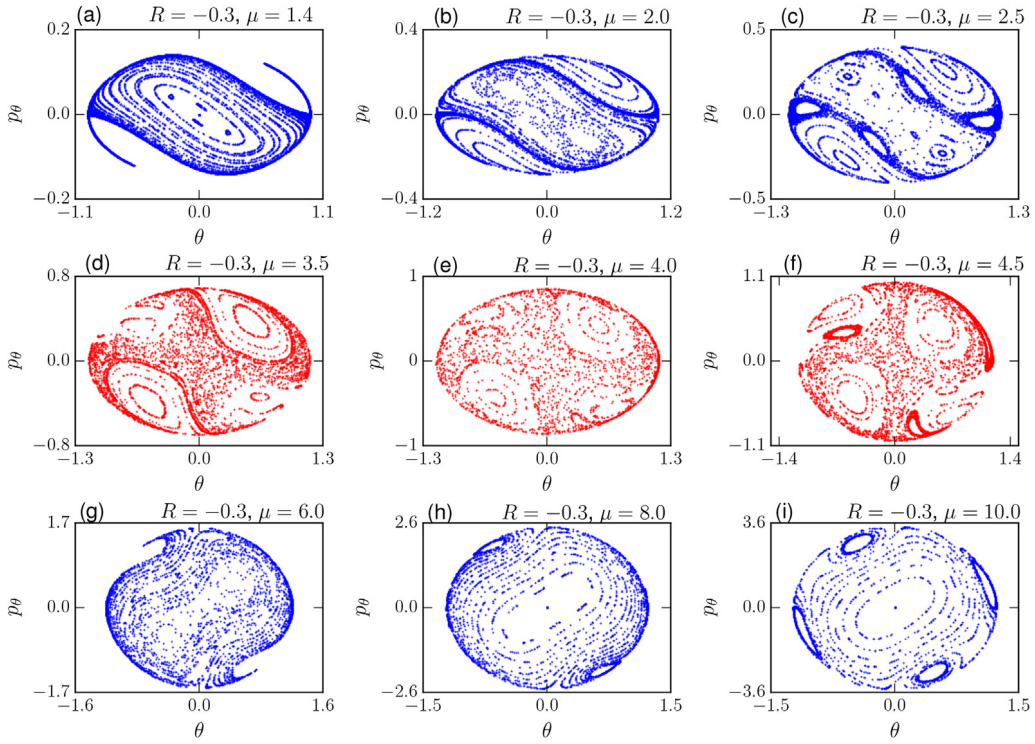

Fig. 9. *Order-chaos-order transition in the PEP at $R = -0.3$ using Eq. (1).* The blue colour indicates the predominantly regular states whereas the red colour highlights the widespread chaos. (For interpretation of the references to colour in this figure legend, the reader is referred to the web version of this article.)

of the torus (on which the initial condition has been chosen) is accompanied by the change in the location of both the minimum and the maximum values of δr.

4. Discussion and conclusions

To conclude, we have explored the order-chaos-order phenomenon in the PEP in detail by working with the truncated Hamiltonian having up to fourth order terms. Before using the Hamiltonian for our purpose, we have systematically justified that it is the minimal and optimal Hamiltonian to work with. While it is desirable that one uses the full Hamiltonian to explain the mechanism behind the order-chaos-order transition both in the libration and the rotation regimes (recall Fig. 2), it is not an analytically feasible exercise. In view of this, our results are quite important because it clearly sheds first light on the exact mechanism of the order-chaos-order in one of the prototype system, viz., the PEP. The fact that it is the overlap between the primary $2:1$ and the secondary $2:1$ resonances that initiates the order to chaos transition in the order-chaos-order phenomenon in the PEP, makes it clear that even if the Chirikov overlap criterion applied to the primary resonances to find widespread chaos fails, there can be the order-chaos-order in the system.

Another well-explored system, which is very similar to the PEP, is the two-degree-of-freedom-spring–mass–pendulum system [41]. An inspection of the system's Hamiltonian, expressed in terms of the action–angle variables of the pendulum and the Hookian spring, shows $2:1$ primary resonance that is known to be responsible to the autoparametric resonance in the system. A numerical investigation [40] of the Poincaré sections reveals that even here the primary and the secondary resonances responsible for the order-chaos-order transition are of the same $2:1$ type; additionally, saddle reconnection identical to the case of the PEP is seen in this system at the autoparametric resonance condition. There have been elaborate studies [40,42] of nonlinear normal modes and their bifurcations in the spring–mass–pendulum system. This motivates a similar future investigation of nonlinear normal modes, their bifurcations and – most importantly – their connection with the overlaps of the primary and the secondary resonances for the case of the PEP. In fact, the connection of the bifurcations of the nonlinear normal modes with the overlaps of the resonances is missing even in the literature of the spring–mass–pendulum system.

The surprising coincidence, if at all it is one, that the primary and the secondary resonances responsible for the order-chaos-order transition are of the same type, e.g., $2:1$ for the PEP, can be witnessed in many other systems as well (see Appendix B for another example). Whether there is a systematic reason behind this is an open question. Also, it may be worth to study the implication of the mechanism found for the order-chaos-order transition on the quantized version of the system. Furthermore, one can always extend the investigations done here to encompass the three-degrees-of-freedom elastic pendulum that is used to model some triatomic molecules.

Acknowledgements

The authors thank Anupam Ghosh for the help with numerics and Manohar K. Sharma for the help with the figures. Fruitful discussions with Govind S. Krishnaswami, Tirth Shah, and K. Srihari are also much appreciated. An anonymous referee is also thanked for the suggestions and comments that have improved the presentation of the paper a great deal.

Appendix A. The approximated Hamiltonian

At the autoparametric resonance condition ($\omega_{20} = 2\omega_{10}$) [19,43], the *approximate/truncated* equations of motion for the PEP are given by [44–46]

$$\ddot{x} + \omega_{10}^2 x = -3\omega_{10}^2 xz/l\,, \tag{A.1a}$$

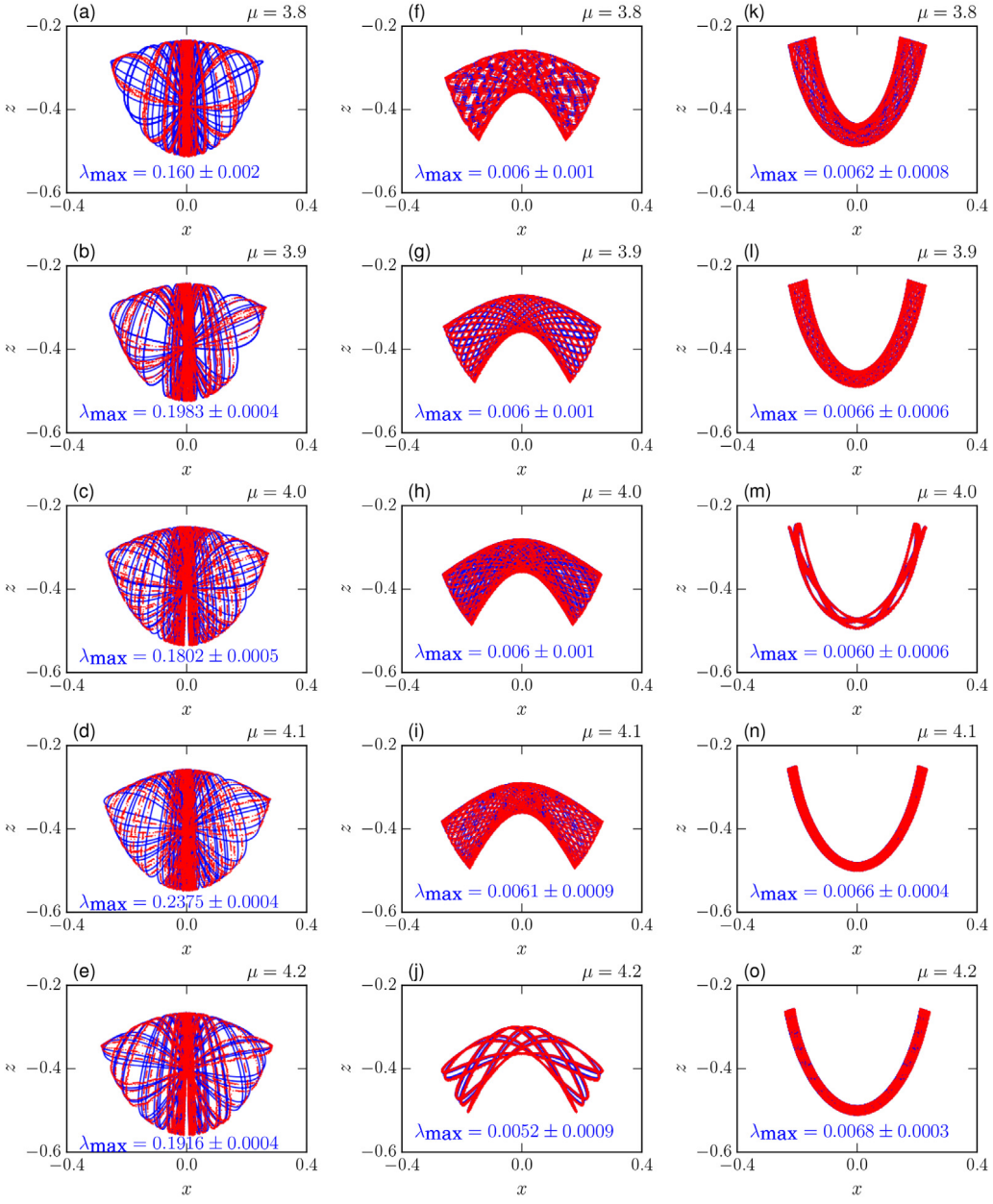

Fig. 10. *Chaotic and quasiperiodic trajectories in the physical x-z space.* This figure presents the chaotic and the quasiperiodic motions for μ ranging from 3.3 to 4.2 at $R = -0.7$. Blue and red trajectories correspond to two nearby initial conditions. First column, i.e., subplots (a)–(e), represent the chaotic trajectories where the blue and the red colours correspond to the initial conditions $(\theta, p_\theta, \delta r) = (0.01, 0.01, 0.0)$ and $(\theta, p_\theta, \delta r) = (0.011, 0.01, 0.0)$ respectively. The second column (subplots (f)–(j)) and the third column (subplots (k)–(o)) respectively depict the quasiperiodic trajectories near the primary 2 : 1 and the secondary 2 : 1 resonances. For the primary 2 : 1 resonance, (0.40, 0.40, 0.0) and (0.401, 0.40, 0.0) are the initial conditions for the blue and the red trajectories respectively, whereas for the secondary 2 : 1 resonance, (−0.40, 0.40, 0.0) and (−0.401, 0.40, 0.0) are the initial conditions for the blue and the red trajectories respectively. The values of the maximum Lyapunov exponent for all the trajectories in blue are mentioned inside the respective subplots. (For interpretation of the references to colour in this figure legend, the reader is referred to the web version of this article.)

$$\ddot{z} + 4\omega_{10}^2 z = -3\omega_{10}^2 x^2/2l\,. \tag{A.1b}$$

This corresponds to the Hamiltonian truncated at the third order, i.e.,

$$H = \frac{1}{2m}({p_x}^2 + {p_z}^2) + \frac{1}{2}m\omega_{10}^2 x^2 + \frac{1}{2}m\omega_{20}^2 z^2 + m\nu_1 x^2 z. \tag{A.2}$$

One further notes [46] that the solutions for x and z assumed to be

$$x(t) = A(t)\cos(\omega_{10}t + \delta_x(t))\,, \tag{A.3a}$$
$$z(t) = B(t)\cos(2\omega_{10}t + \delta_z(t))\,, \tag{A.3b}$$

having the sinusoidal functions with slowly varying amplitudes and phases, yields the following flow equations:

$$\dot{A} = -\frac{3\omega_{10}AB}{4l}\sin\chi\,, \tag{A.4a}$$
$$\dot{B} = \frac{3\omega_{10}A^2}{16l}\sin\chi\,, \tag{A.4b}$$
$$\dot{\chi} = \frac{3\omega_{10}}{2l}\left(\frac{A^2}{8B} - B\right)\cos\chi\,. \tag{A.4c}$$

Here, $\chi \equiv \delta_z - 2\delta_x$. It is easy to verify that the flow equations possess two constants of motion, viz., $A^2 + 4B^2$ and $A^2 B\cos\chi$, making the (approximated) dynamical system mostly non-chaotic. In fact,

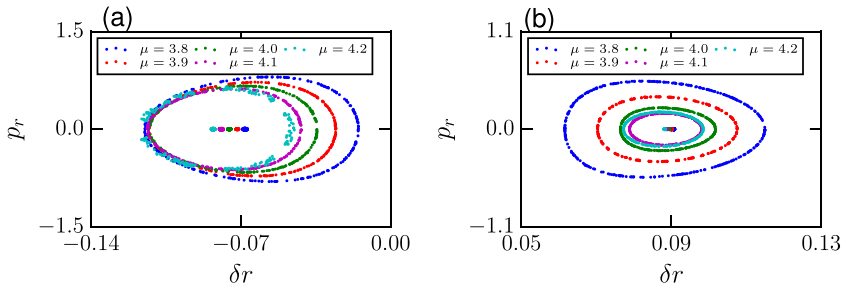

Fig. 11. *Resonance centres and nearby quasiperiodic orbits in δr-p_r plane.* Blue, red, green, magenta, and cyan colours respectively correspond to $\mu = 3.8$, 3.9, 4.0, 4.1, and 4.2 respectively. Subplot (a) shows that the torus, for the initial condition chosen in the primary 2 : 1 resonance island, shrinks from the right side with increasing μ. In contrast, subplot (b) shows that the torus, for the initial condition chosen in the secondary 2 : 1 resonance island, shrink along both the left and the right side, as μ increases.

even the elastic pendulum is integrable if we keep only up to cubic terms [47].

Hence, we conclude that in order to be able to easily see chaos in the system, it is pertinent that the Hamiltonian should be approximated such that at least the terms up to fourth order are retained, i.e.,

$$H = \frac{1}{2m}({p_x}^2 + {p_z}^2) + \frac{1}{2}m\omega_{10}^2x^2 + \frac{1}{2}m\omega_{20}^2z^2 + m\nu_1x^2z + \frac{1}{4}m\nu_2x^4 - m\nu_2x^2z^2\,. \tag{A.5}$$

Indeed, on applying any standard perturbation method [43,48–50], we arrive at the following flow equations:

$$\begin{aligned}\dot{A} = {} & -\frac{3\omega_{10}AB}{4l}\sin(\delta_z - 2\delta_x) + \frac{9\omega_{10}AB^2}{64l^2}\cos(\delta_z + \delta_x)\sin(\delta_z - \delta_x) \\ & - \frac{27\omega_{10}AB^2}{64l^2}\cos(\delta_z - \delta_x)\sin(\delta_z + \delta_x) \\ & - \frac{9\omega_{10}AB^2}{16l^2}\cos(\delta_z - \delta_x) \\ & \times \sin(\delta_z - \delta_x) + \frac{9\omega_{10}A^3}{64l^2}\sin 2\delta_x \\ & + \frac{9\omega_{10}A^3}{128l^2}\cos 2\delta_x \sin 2\delta_x\,,\end{aligned} \tag{A.6a}$$

$$\begin{aligned}\dot{\delta_x} = {} & \frac{3\omega_{10}B}{4l}\cos(\delta_z - 2\delta_x) - \frac{9\omega_{10}B^2}{64l^2}\cos(\delta_z + \delta_x)\cos(\delta_z - \delta_x) \\ & - \frac{27\omega_{10}B^2}{64l^2}\sin(\delta_z + \delta_x)\sin(\delta_z - \delta_x) - \frac{9\omega_{10}B^2}{16l^2}\sin^2(\delta_z - \delta_x) \\ & - \frac{21\omega_{10}B^2}{64l^2} + \frac{27\omega_{10}A^2}{128l^2} + \frac{9\omega_{10}A^2}{64l^2}\cos 2\delta_x \\ & - \frac{9\omega_{10}A^2}{128l^2}\sin^2 2\delta_x\,,\end{aligned} \tag{A.6b}$$

$$\begin{aligned}\dot{B} = {} & \frac{3\omega_{10}A^2}{16l}\sin(\delta_z - 2\delta_x) + \frac{9\omega_{10}A^2B}{128l^2}\cos(\delta_z + \delta_x)\sin(\delta_x - \delta_z) \\ & + \frac{27\omega_{10}A^2B}{128l^2}\sin(\delta_z + \delta_x)\cos(\delta_x - \delta_z) \\ & + \frac{9\omega_{10}A^2B}{32l^2}\cos(\delta_x - \delta_z) \\ & \times \sin(\delta_z - \delta_x)\,,\end{aligned} \tag{A.6c}$$

$$\begin{aligned}\dot{\delta_z} = {} & \frac{3\omega_{10}A^2}{16lB}\cos(\delta_z - 2\delta_x) - \frac{9\omega_{10}A^2}{128l^2}\cos(\delta_z + \delta_x)\cos(\delta_x - \delta_z) \\ & + \frac{27\omega_{10}A^2}{128l^2}\sin(\delta_z + \delta_x)\sin(\delta_x - \delta_z) + \frac{9\omega_{10}A^2}{32l^2}\sin(\delta_z - \delta_x) \\ & \times \sin(\delta_x - \delta_z) - \frac{3\omega_{10}A^2}{8l^2}\,.\end{aligned} \tag{A.6d}$$

We validate numerically that this indeed is a chaotic system. As an illustration, we remark that using the initial condition, $A(0) = 5.523$, $B(0) = 0.805$, $\delta_x(0) = -\pi/2$, $\delta_z(0) = \pi$, the maximum Lyapunov exponent is found out to be $+3.539 \pm .001$.

To conclude, it suffices for the purpose of the paper to work with the Hamiltonian approximated to keep terms only up to the fourth-order, i.e., with the equations of motion that have nonlinearity up to the cubic order.

Appendix B. Chaos to order transition in the generalized Hénon–Heiles systems

As pointed out in the introduction, there are several other systems that undergo the order-chaos-order transition. In this appendix, we have shown that the generalized Hénon–Heiles system [9] also exhibits the transition and that transition is due to overlap of a primary and a secondary resonance of the same type, viz., 2 : 2. The Hamiltonian for the generalized Hénon–Heiles system is,

$$H = \frac{p_x^2}{2} + \frac{p_y^2}{2} + \frac{1}{2}ax^2 + \frac{1}{2}ay^2 + cx^4 + cy^4 + bx^2y - \frac{1}{3}by^3 + 2cx^2y^2\,. \tag{B.1}$$

Let the action–angle variables of the unperturbed systems be $(\phi_x^0, \phi_y^0, J_x^0, J_y^0)$, so that

$$x = \sqrt{\frac{2J_x^0}{\sqrt{a}}}\sin\phi_x^0\,, \tag{B.2a}$$

$$p_x = \sqrt{2J_x^0\sqrt{a}}\cos\phi_x^0\,, \tag{B.2b}$$

$$y = \sqrt{\frac{2J_y^0}{\sqrt{a}}}\sin\phi_y^0\,, \tag{B.2c}$$

$$p_y = \sqrt{2J_y^0\sqrt{a}}\cos\phi_y^0\,. \tag{B.2d}$$

The Hamiltonian of this system in terms of the action angle variable is, therefore,

$$\begin{aligned}H = {} & \sqrt{a}\left(J_x^0 + J_y^0\right) - \frac{b}{3}\left(\frac{2J_y^0}{\sqrt{a}}\right)^{\frac{3}{2}}\sin^3\phi_y^0 + 4c\left(\frac{{J_x^0}^2}{a}\sin^4\phi_x^0 \right. \\ & \left. + \frac{{J_y^0}^2}{a}\sin^4\phi_y^0\right) \\ & + \frac{b}{2}\frac{J_x^0}{\sqrt{a}}\left(\frac{2J_y^0}{\sqrt{a}}\right)^{\frac{1}{2}}\left[2\sin\phi_y^0 - \sin(2\phi_x^0 + \phi_y^0)\right. \\ & \left. + \sin(2\phi_x^0 - \phi_y^0)\right] + c\frac{J_x^0}{\sqrt{a}}\frac{J_y^0}{\sqrt{a}}\end{aligned}$$

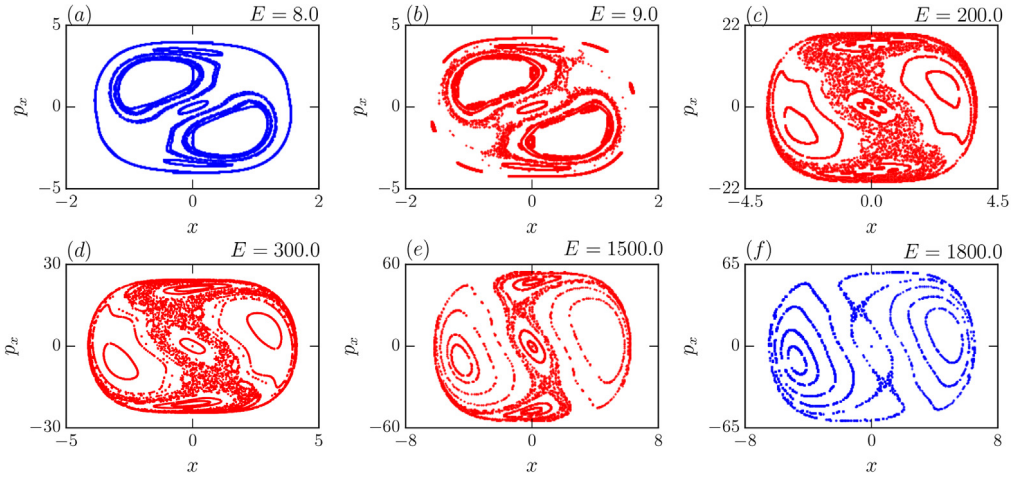

Fig. B.12. *Order-chaos-order phenomena in the generalized Hénon–Heiles system.* Above figure shows the Poincaré sections of the system in x-p_x plane. The blue plots represent the system in the predominantly ordered states and the red plots highlight the widespread chaos in the system. The transition from order to chaos is observed at $E \approx 9$ due to the overlap of the 2 : 2 primary resonance and the 2 : 2 secondary resonance. We observe another transition from the chaotic to the ordered state at energy $E \approx 1800$. Here, $a = 1$, $b = \sqrt{10}$, and $c = 1$. (For interpretation of the references to colour in this figure legend, the reader is referred to the web version of this article.)

$$\times \left[2 - 2\cos 2\phi_x^0 - 2\cos 2\phi_y^0 - \cos(2\phi_x^0 + 2\phi_y^0) - \cos(2\phi_x^0 - 2\phi_y^0)\right]. \tag{B.3}$$

From the Hamiltonian, it is clear that there are only 2 : 1 and 2 : 2 primary resonances in the system ($\sqrt{a} > 0$). This system, unfortunately, is not easily amenable to the Chirikov overlap technique because the unperturbed (quadratic) part of the Hamiltonian is neither non-degenerate nor iso-energetically non-degenerate. Nevertheless, Fig. B.12 illustrates the order-chaos-order transition in the system and establishes that it is mainly due to the interaction between the primary 2 : 2 and the secondary 2 : 2 resonances.

References

[1] J.H. Lowenstein, Essentials of Hamiltonian Dynamics, Cambridge University Press, Cambridge, 2012, http://dx.doi.org/10.1017/CBO9780511793721.

[2] N.J. Fitch, C.A. Weidner, L.P. Parazzoli, H.R. Dullin, H.J. Lewandowski, Experimental demonstration of classical hamiltonian monodromy in the 1 : 1 : 2 resonant elastic pendulum, Phys. Rev. Lett. 103 (2009) 034301, http://dx.doi.org/10.1103/PhysRevLett.103.034301, URL https://link.aps.org/doi/10.1103/PhysRevLett.103.034301.

[3] B.P. Winnewisser, M. Winnewisser, I.R. Medvedev, M. Behnke, F.C. De Lucia, S.C. Ross, J. Koput, Experimental confirmation of quantum monodromy: The millimeter wave spectrum of cyanogen isothiocyanate ncncs, Phys. Rev. Lett. 95 (2005) 243002, http://dx.doi.org/10.1103/PhysRevLett.95.243002, URL https://link.aps.org/doi/10.1103/PhysRevLett.95.243002.

[4] R.H. Cushman, H.R. Dullin, A. Giacobbe, D.D. Holm, M. Joyeux, P. Lynch, D.A. Sadovskií, B.I. Zhilinskií, CO_2 Molecule as a quantum realization of the 1 : 1 : 2 resonant swing-spring with monodromy, Phys. Rev. Lett. 93 (2004) 024302, http://dx.doi.org/10.1103/PhysRevLett.93.024302, URL https://link.aps.org/doi/10.1103/PhysRevLett.93.024302.

[5] H. Dullin, A. Giacobbe, R. Cushman, Monodromy in the resonant swing spring, Physica D 190 (1) (2004) 15–37, http://dx.doi.org/10.1016/j.physd.2003.10.004, URL http://www.sciencedirect.com/science/article/pii/S0167278903004081.

[6] A. Giacobbe, R.H. Cushman, D.A. Sadovskií, B.I. Zhilinskií, Monodromy of the quantum 1:1:2 resonant swing spring, J. Math. Phys. 45 (12) (2004) 5076–5100, http://dx.doi.org/10.1063/1.1811788.

[7] Z. Deng, F.T. Hioe, Chaos-order-chaos transitions in a two-dimensional Hamiltonian system, Phys. Rev. Lett. 56 (1986) 1757, http://dx.doi.org/10.1103/PhysRevLett.56.1757.3.

[8] J. Reichl, H. Büttner, Stochastic and regular motion in a four-particle system, Phys. Rev. A 33 (1986) 2184–2185, http://dx.doi.org/10.1103/PhysRevA.33.2184.

[9] Y. Bolotin, V. Gonchar, V. Tarasov, N. Chekanov, The transition regularity-chaos-regularity and statistical properties of energy spectra, Phys. Lett. A 135 (1989) 29–31, http://dx.doi.org/10.1016/0375-9601(89)90720-2.

[10] J.P. van der Weele, E. de Kleine, The order—chaos—order sequence in the spring pendulum, Physica A 228 (1996) 245–272, http://dx.doi.org/10.1016/0378-4371(95)00426-2.

[11] G.S. Krishnaswami, H. Senapati, Classical three rotor problem: periodic solutions, stability and chaos, 2018, ArXiv e-prints arXiv:1811.05807.

[12] J.H. Heinbockel, R.A. Struble, Resonant oscillations of an extensible pendulum, Z. Angew. Math. Phys. 14 (1963) 262–269, http://dx.doi.org/10.1007/BF01601064.

[13] T.R. Kane, M.E. Kahn, On a class of two-degree-of-freedom oscillations, J. Appl. Mech. 35 (1968) 547–552, http://dx.doi.org/10.1115/1.3601249.

[14] D.L. Hitzl, The swinging spring - Families of periodic solutions and their stability. I, Astron. Astrophys. 40 (1975) 147–159.

[15] D.L. Hitzl, The swinging spring - approximate analyses for low and very high energy. II, Celest. Mech. 12 (3) (1975) 359–382, http://dx.doi.org/10.1007/bf01228569.

[16] D.L. Hitzl, The swinging spring - Invariant curves formed by quasi-periodic solutions. III, Astron. Astrophys. 41 (1975) 187–198.

[17] Y. Narkis, On the stability of a spring-pendulum, Z. Angew. Math. Phys. 28 (1977) 343–348, http://dx.doi.org/10.1007/BF01595601.

[18] T.E. Cayton, The laboratory spring–mass oscillator: an example of parametric instability, Amer. J. Phys. 45 (1977) 723–732, http://dx.doi.org/10.1119/1.11035.

[19] L. Falk, Recurrence effects in the parametric spring pendulum, Amer. J. Phys. 46 (1978) 1120–1123, http://dx.doi.org/10.1119/1.11152.

[20] M.G. Rusbridge, Motion of the sprung pendulum, Amer. J. Phys. 48 (1980) 146–151, http://dx.doi.org/10.1119/1.12190.

[21] B.A. Aničin, D.M. Davidović, V.M. Babović, On the linear theory of the elastic pendulum, Eur. J. Phys. 14 (1993) 132, URL http://stacks.iop.org/0143-0807/14/i=3/a=007.

[22] R. Carretero-Gonzalez, H.N. Nunez-Yepez, A.L. Salas-Brito, Regular and chaotic behaviour in an extensible pendulum, Eur. J. Phys. 15 (1994) 139, URL http://stacks.iop.org/0143-0807/15/i=3/a=009.

[23] T.Y. Petrosky, Chaos and irreversibility in a conservative nonlinear dynamical system with a few degrees of freedom, Phys. Rev. A 29 (1984) 2078–2091, http://dx.doi.org/10.1103/PhysRevA.29.2078, URL https://link.aps.org/doi/10.1103/PhysRevA.29.2078.

[24] A. Lichtenberg, M. Lieberman, Regular and Chaotic Dynamics, Springer-Verlag, New York, 1992.

[25] A.N. Kolmogorov, On the preservation of quasi periodic motions under a small variation of hamilton's function, Dokl. Akad. Nauk. SSSR 98 (1954) 525.

[26] J.K. Moser, On invariant curves of area-preserving mappings of an annulus, Nach. Akad. Wiss. Göttingen, Math. Phys. K1. II 1 (1962) 1–20.

[27] V.I. Arnol'd, Small denominators and problems of stability of motion in classical and celestial mechanics, Russ. Math. Surv. 18 (6) (1963) 85, URL http://stacks.iop.org/0036-0279/18/i=6/a=R02.

[28] V.I. Arnold, Instability of dynamical systems with many degrees of freedom, Dokl. Akad. Nauk. SSSR 156 (6) (1964) 9–12.

[29] B.V. Chirikov, A universal instability of many-dimensional oscillator systems, Phys. Rep. 52 (5) (1979) 263–379, http://dx.doi.org/10.1016/0370-1573(79)90023-1, URL http://www.sciencedirect.com/science/article/pii/0370157379900231.

[30] R.H. Cushman, L.M. Bates, The spherical pendulum, in: Global Aspects of Classical Integrable Systems, Birkhäuser, Basel, 1997, pp. 147–186.
[31] A.J. Maciejewski, M. Przybylska, J.-A. Weil, Non-integrability of the generalized spring-pendulum problem, J. Phys. A 37 (7) (2004) 2579, URL http://stacks.iop.org/0305-4470/37/i=7/a=005.
[32] M. Tabor, Chaos and Integrability in Nonlinear Dynamics: An Introduction, Wiley, New York, NY, 1989.
[33] D.F. Lawden, Elliptic Functions and Applications, Springer-Verlag, New York, 1989.
[34] A. Kiper, Fourier series coefficients for powers of the jacobian elliptic functions, Math. Comp. 43 (167) (1984) 247–259.
[35] G.H. Walker, J. Ford, Amplitude instability and ergodic behavior for conservative nonlinear oscillator systems, Phys. Rev. 188 (1969) 416–432, http://dx.doi.org/10.1103/PhysRev.188.416.
[36] G.H. Walker, Amplitude instabilities in systems of nonlinear coupled oscillators (Ph.D. thesis), Georgia Institute of Technology, Atlanta, 1968.
[37] D.W. Oxtoby, S.A. Rice, Nonlinear resonance and stochasticity in intramolecular energy exchange, J. Chem. Phys. 65 (1976) 1676–1683, http://dx.doi.org/10.1063/1.433301.
[38] J.M. Greene, A method for determining a stochastic transition, J. Math. Phys. 20 (6) (1979) 1183–1201, http://dx.doi.org/10.1063/1.524170.
[39] M. de Sousa, F. Marcus, I. Caldas, R. Viana, Energy distribution in intrinsically coupled systems: The spring pendulum paradigm, Physica A 509 (2018) 1110–1119.
[40] F. Wang, A.K. Bajaj, K. Kamiya, Nonlinear normal modes and their bifurcations for an inertially coupled nonlinear conservative system, Nonlinear Dynam. 42 (3) (2005) 233–265.
[41] H. Hatwal, A. Mallik, A. Ghosh, Non-linear vibrations of a harmonically excited autoparametric system, J. Sound Vib. 81 (2) (1982) 153–164.
[42] C. Pak, Nonlinear Normal Mode Dynamics: For Two Degree-of-Freedom Systems, Inha University Press, 1999.
[43] A.H. Nayfeh, Perturbation Methods, Wiley-VCH Verlag GmbH, Berlin, 2000.
[44] M.G. Olsson, Why does a mass on a spring sometimes misbehave?, Amer. J. Phys. 44 (1976) 1211–1212, http://dx.doi.org/10.1119/1.10265.
[45] E. Breitenberger, R.D. Mueller, The elastic pendulum: A nonlinear paradigm, J. Math. Phys. 22 (1981) 1196–1210, http://dx.doi.org/10.1063/1.525030.
[46] H.M. Lai, On the recurrence phenomenon of a resonant spring pendulum, Amer. J. Phys. 52 (1984) 219–223, http://dx.doi.org/10.1119/1.13696.
[47] P. Lynch, Resonant motions of the three-dimensional elastic pendulum, Int. J. Non-Linear Mech. 37 (2) (2002) 345–367, http://dx.doi.org/10.1016/S0020-7462(00)00121-9, URL http://www.sciencedirect.com/science/article/pii/S0020746200001219.
[48] A. Sarkar, J.K. Bhattacharjee, S. Chakraborty, D.B. Banerjee, Center or limit cycle: renormalization group as a probe, Eur. Phys. J. D 64 (2) (2011) 479–489, http://dx.doi.org/10.1140/epjd/e2011-20060-1.
[49] L.-Y. Chen, N. Goldenfeld, Y. Oono, Renormalization group and singular perturbations: Multiple scales, boundary layers, and reductive perturbation theory, Phys. Rev. E 54 (1996) 376–394, http://dx.doi.org/10.1103/PhysRevE.54.376, URL https://link.aps.org/doi/10.1103/PhysRevE.54.376.
[50] J.K. Bhattacharjee, A.K. Malik, S. Chakraborty, An introduction to non-linear oscillators: a pedagogical review, Indian J. Phys. 81 (2007) 1115.